ANNALS of Clinical and Translational Neurology
Open Access
ANA American Neurological Association since 1875

BRIEF COMMUNICATION

P5CS expression study in a new family with *ALDH18A1*-associated hereditary spastic paraplegia SPG9

Pamela Magini[1,*], Clara Marco-Marin[2,3,*], Juan M. Escamilla-Honrubia[2,3], Diego Martinelli[4], Carlo Dionisi-Vici[4], Francesca Faravelli[5], Francesca Forzano[6], Marco Seri[1,7], Vicente Rubio[2,3] & Emanuele Panza[1,7]

[1]Medical Genetics Unit, S. Orsola-Malpighi Hospital, Bologna, Italy
[2]Instituto de Biomedicina de Valencia of the CSIC, Valencia, Spain
[3]Centro para Investigación Biomédica en Red sobre Enfermedades Raras CIBERER-ISCIII, Valencia, Spain
[4]Division of Metabolism, Bambino Gesù Children's Research Hospital, Rome, Italy
[5]Clinical Genetics, NE Thames Regional Genetics Service, Great Ormond Street Hospital for Children, NHS Foundation Trust, London, United Kingdom
[6]Clinical Genetics Department, SE Thames Regional Genetics Service, Guy's & St Thomas' NHS Foundation Trust, London, United Kingdom
[7]Department of Medical and Surgical Sciences, University of Bologna, Bologna, Italy

Correspondence
Marco Seri and Emanuele Panza, Department of Medical and Surgical Sciences, S. Orsola-Malpighi University Hospital, University of Bologna, Via Massarenti 9, Bologna Italy. Tel: +39 051 2088421; Fax: +39 051 2088416; E-mails: marco.seri@unibo.it and emanuele.panza@unibo.it
and
Vicente Rubio, Instituto de Biomedicina de Valencia (IBV-CSIC) and CIBERER-ISCIII, Jaime Roig 11, Valencia-46010, Spain. Tel: +34 963391772; Fax: +34 963690800; E-mail: rubio@ibv.csic.es

Funding information
Whole-exome sequencing analysis was funded by a "Fondazione del Monte" grant to Professor MS for clinical exome sequencing applied to the diagnosis of ultrarare/orphan inherited diseases. The Genetic Bank (Biobanca del Laboratorio di Genetica Umana IRCCS Gaslini), member of the Network Telethon of Genetic Biobanks (Project No. GTB12001), funded by Telethon Italy, provided us with specimens. VR was supported by grants of the Fundación Inocente Inocente and of the Spanish Government (MINECO BFU2017-84264-P).

Received: 2 March 2019; Revised: 14 May 2019; Accepted: 28 May 2019

Annals of Clinical and Translational Neurology **2019; 6(8): 1533–1540**

doi: 10.1002/acn3.50821

*These authors contributed equally to this work.

Abstract

In 2015–2016, we and others reported *ALDH18A1* mutations causing dominant (SPG9A) or recessive (SPG9B) spastic paraplegia. In vitro production of the *ALDH18A1* product, Δ^1-pyrroline-5-carboxylate synthetase (P5CS), appeared necessary for cracking SPG9 disease-causing mechanisms. We now describe a baculovirus–insect cell system that yields mgs of pure human P5CS and that has proven highly valuable with two novel P5CS mutations reported here in new SPG9B patients. We conclude that both mutations are disease-causing, that SPG9B associates with partial P5CS deficiency and that it is clinically more severe than SPG9A, as reflected in onset age, disability, cognitive status, growth, and dysmorphic traits.

Introduction

ALDH18A1 gene-related spastic paraplegias (SPG9A and SPG9B) are extremely rare disorders recognized quite recently.[1,2] They are due to mutations in *ALDH18A1* (Fig. 1A), which encodes Δ^1-pyrroline-5-carboxylate synthetase (P5CS), an enzyme that catalyzes the initial two steps of ornithine and proline biosynthesis.[3,4] This bifunctional single-chain homo-oligomeric[2] protein is composed of glutamate 5-kinase (G5K) and glutamyl-5-phosphate (G5P) reductase (G5PR) components[3] (Fig. 1A). Biallelic *ALDH18A1* mutations were known to cause a cutis laxa neurocutaneous syndrome[5,6] (ARCL3A, MIM#219150). In 2015–2016, we and others[1,2] reported *ALDH18A1* mutations in dominant complicated spastic paraplegia (SPG9A, MIM#601162). A recessive form of SPG9 (SPG9B) associated to biallelic *ALDH18A1* mutations was also reported[1] (SPG9B, MIM#616586). The effects of *ALDH18A1*-related disease mutations appear to result from loss of P5CS[7–9]/decrease of P5CS function[1,2,5,6,10–12], leading to the proposal that dominant mutations cause *ALDH18A1* pathologies by a dominant negative effect[2,11,12]. Similarly to Charcot-Marie-Tooth disease due to *GDAP1* gene mutations[13], it is conceivable that dominant SPG9 mutations could cause a less severe disease phenotype than biallelic recessive ones.

If disease severity in SPG9 has to be correlated with P5CS enzyme activity, it is crucial to have a procedure for directly testing the mutations' effects on P5CS activity and stability. We describe here this procedure for in vitro production of pure P5CS using an engineered baculovirus–insect cell system, exemplifying the value of this system with two novel *ALDH18A1* mutations found in a new family of SPG9B that is also reported here. In addition, we rationalize the observed effects of these mutations using the crystal structure (Protein Database, PDB, entry 2H5G) of the G5PR component of human P5CS. Furthermore, by expanding by one family the meager (just 6 prior families)[1,9,14,15] SPG9B database, we conclude on sound bases that SPG9B is generally more severe than SPG9A.

Materials and Methods

See Supplementary Methods for details.

Production of human P5CS

An engineered baculovirus was prepared[16–18] (Fig. 1B) by co-transfection of Sf9 cells with bacmid DH10:KO1629 and with a pOPINM plasmid (Clontech) bearing the mature human P5CS coding sequence (Fig. S1). This virus was used for production in Sf9 insect cells of P5CS preceded by a His_6-MBP-3C protease cleavable double tag[17]. Clinical mutations were introduced by site-directed mutagenesis of the pOPINM derivative carrying the P5CS

Figure 1. Human P5CS, its "in vitro" production and assay in wild-type and mutant forms, and structure-based inferences. (A) Linear scheme of the composition of the P5CS polypeptide, with the N-terminal mitochondrial targeting sequence in yellow, the G5K component in white and the cofactor-binding, catalytic and oligomerization domains of the G5PR component in blue, red, and gray, respectively. The different mutations (single letter amino acid code) reported in SPG9A (blue) and SPG9B (red), including the two mutations reported here (yellow banners) are mapped. The two residues spliced out in the short form of P5CS, and the catalytic Cys612 of the G5PR domain are mapped and labeled in green. The reactions catalyzed are shown below the corresponding components, and the role of the two reactions in the synthesis of proline, ornithine (and arginine and urea) are also schematized. OAT, ornithine transcarbamylase; PYCR1, pyrrolin-5-carboxylate reductase. (B) Diagram schematizing the production and purification of recombinant human P5CS using a baculovirus/insect cell system. Sodium dodecyl sulphate-polyacrylamide gel electrophoresis (SDS-PAGE, 10% polyacrylamide gel, with Coomasie staining) of the enzyme preparations produced and used in these studies is shown. The band corresponding to P5CS, as well as to traces of residual uncleaved MBP-tagged P5CS and free MBP tag are identified. St, protein markers, with masses given in kDa on the side. The values under the tracks give (means ± SE; *n* of 2–4 for each form) the yield of purified protein and the specific activities in the global P5CS reaction and the partial G5K reaction. (C) Dependency of G5PR activity of wild type or mutant forms on the concentration of *Escherichia coli* G5K (top graph), added as a source of G5P, or on the concentration of NADPH (bottom graph). (D) Thermofluor assays (means of three experiments) for purified wild type (WT) and mutant P5CS forms. Addition of 0.2 mmol/L NADPH did not alter the thermofluor profiles of these three protein forms (data not shown). The broken line shows the unfolding profile for isolated MBP, to show that the profiles observed with P5CS are not due to the traces of free MBP present in the sample. T_m values are indicated with interrupted straight lines. (E) Structure of the human G5PR component of P5CS (PDB file 2H5G), mapping therein the residues that are mutated in the present patients. Drawings are cartoon representations, with blue coloring of the cofactor-binding domain and the β hairpin emerging from it as a part of the oligomerization domain; and with red coloring of the catalytic domain and the C-terminal extension of this domain that ends as the two final strands of the oligomerization domain. To localize the substrate-binding sites, NADP has been placed instead of NAD after superimposition of the NAD-bound cofactor binding domain of ALDH (PDB 1AD3) on this domain of human G5PR. To localize the amino acid site, the α-aminoadipate of the homologous enzyme α-aminoadipate dehydrogenase has been placed on the equivalent location of G5PR by superimposing the subunit of this enzyme in the α-aminoadipate-bound form (PDB 4ZUL) with the human G5PR subunit structure. These ligands are shown in semitransparent spheres representation, with C, P, O and N atoms colored gray, magenta, red, and blue, respectively. In the upper panel, a subunit is shown (residues Arg375 and Ser497 in yellow spheres, and Cys612 as a cyan sphere), zooming in the middle panel on the hydrophobic nest around Ser497 (amino acids side-chains in sticks; broken line, a hydrogen bond), while the bottom panel shows the dimer, illustrating the Arg371-Asp715 intersubunit salt bridge.

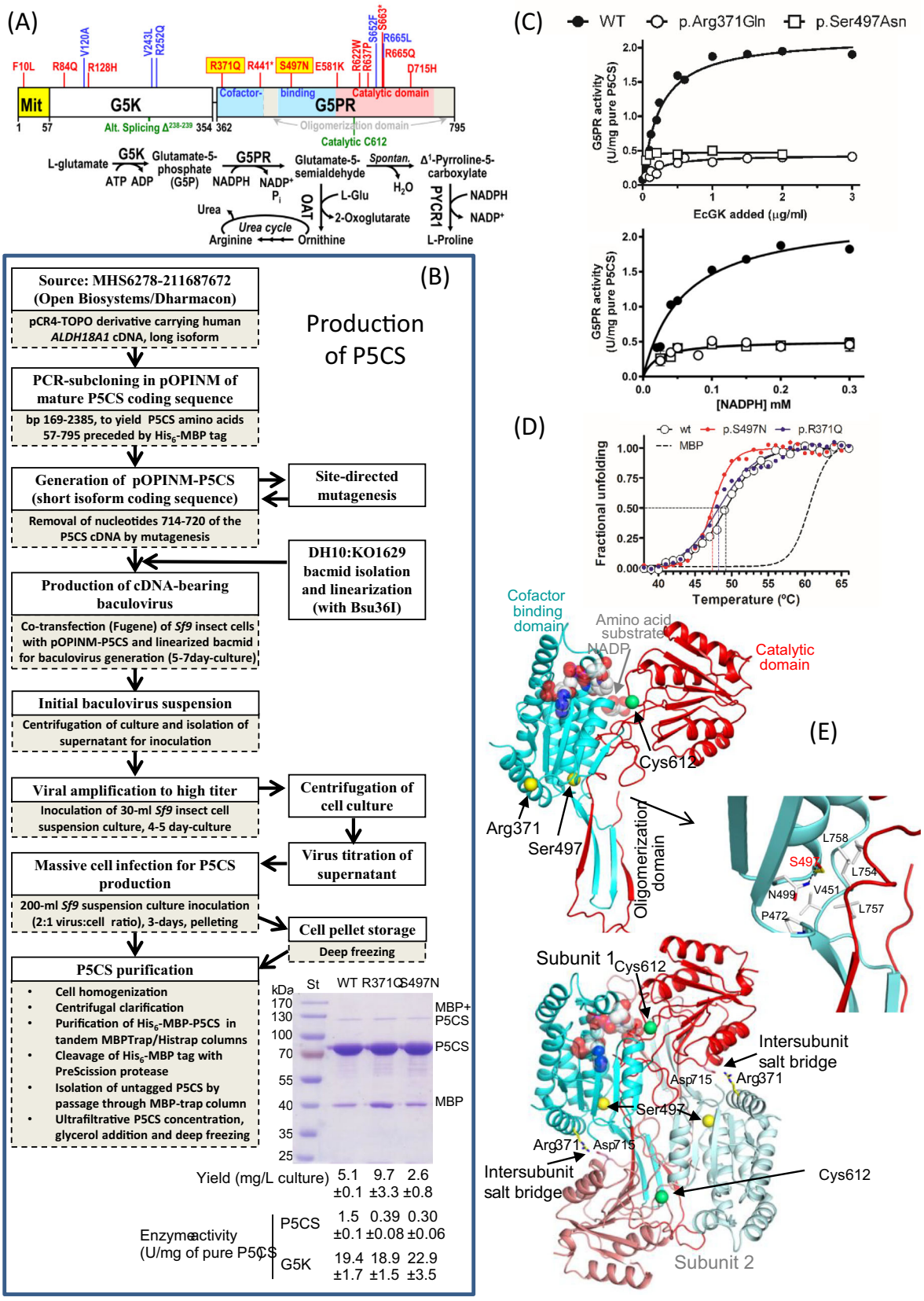

(A)

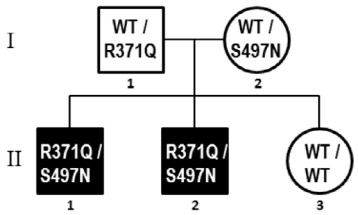

(B)

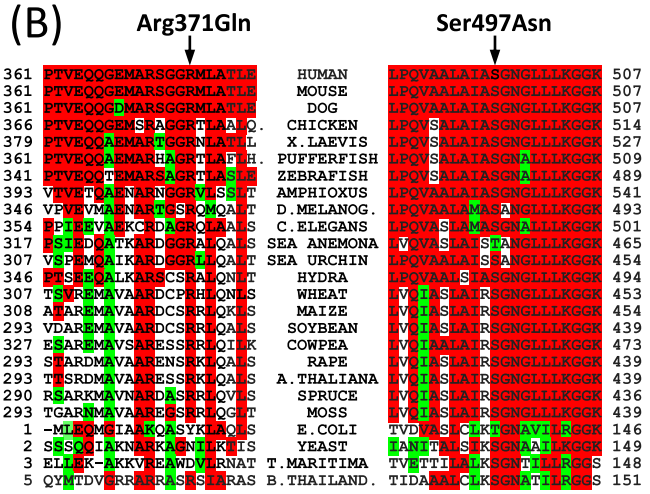

(C)

	SPG9B	SPG9A
Families	7	7
Patients	15	38
Mutations	12	5
Presentation	Familial	Familial (2 sporadic)
Disease manifestations	**% of the reported patients / % of the reported families**	
Onset	Late onset	Very late onset
Dysmorphic facies	55% / 43%	Not reported
Growth retardation	40% / 43%	13% /29%
Microcephaly	47% / 43%	Not reported
Cognitive impairment	Constant	5% / 29%
Seizures	20% / 43%	3% /14%
Motor disability, gait	Constant. Progress to ambulation loss	Constant. Less severe than SPG9B
Cataracts/ corneal cloud	13% / 29%	50% / 57%

(D)

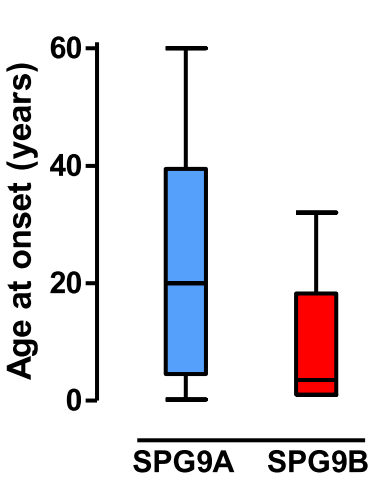

Figure 2. SPG9B family tree, conservation of the mutated residues and comparison of the phenotypes of dominant and recessive forms of SPG9. (A) The distribution of mutations (single-letter amino acid notation; WT, wild-type allele) in the family tree supports recessive inheritance. Squares, males; circles, females. Black filling denotes a diseased individual. (B) Amino acid (single-letter code) sequence of the regions hosting the mutations, aligned with the corresponding regions of P5CS of other species or with microbial monofunctional G5PR. Identities are highlighted in red and conservative replacements in green. In the species names, the following abbreviations have been used: X., *Xenopus*; D., *Drosophila*; C., *Caenorhabditis*; RAPE, rapeseed; E., *Escherichia*; T., *Thermotoga*; B. THAILAND, *Burkholderia thailandensis*. (C) Comparison of important disease traits in the patients reported of SPG9A[1,2] or of SPG9B[1,9,14,15], including those reported here. The number of patients, families, and mutations are given on the top part. The colors from dark red to light reddish and blue reflect progressively decreasing frequencies (red hues) or not occurrence (blue) of a given manifestation, noting in each square the frequencies (as %) with which a given clinical feature was reported in the published patients and families of SPG9A and SPG9B. (D) Box plot summarizing the ages of disease onset for patients with SPG9A or SPG9B. The box encompases the range between the first and the third quartile, and the whiskers define the entire range. The horizontal line within the box is the median.

cDNA. Doubly-tagged P5CS purified by tandem affinity chromatography with MBP- and His-trap columns (GE Healthcare) was freed from both tags by PreScission protease (GE Healthcare) digestion followed by nontagged P5CS isolation by a final affinity chromatography step.

Enzyme activity and stability assays

Spectrophotometric activity assays at 25°C were used[2], monitoring at 340 nm the oxidation of either NADPH in the complete P5CS reaction or the G5PR partial reaction;

or the oxidation of NADH in the G5K partial reaction, coupling ADP production to NADH oxidation using pyruvate kinase and lactate dehydrogenase.

Thermofluor assays[19] were used to monitor P5CS protein unfolding with increasing temperature (1°C increase/min). Here, T_m is the temperature giving a fluorescence increase of 50% of the maximum increase attained.

Clinical and genetic studies

Consent was obtained for DNA sequencing, for using the results in research, and for this publication. Retrospective clinical and laboratory information gathered for patient care was used, precluding the need for ethics committee approval. We complied with the ethical principles of the Helsinki Declaration.

Biallelic *ALDH18A1* mutations were identified in the index patient by whole-exome sequencing (WES). Sanger sequencing (Fig. S2) was used for confirmation and for familial segregation analysis.

Results and Discussion

See also Supplementary Results.

Production of recombinant human P5CS

We recombinantly produced human P5CS as schematized in Figure 1B in an engineered baculovirus–insect cell system. The doubly-tagged P5CS produced could be purified easily by tandem affinity chromatography followed by tag removal (PreScission protease) and a second round of affinity purification that frees P5CS from residual non-cleaved tagged P5CS and from the excised tags. Using this approach, mg amounts of homogeneous largely pure (Fig. 1B, bottom image and yield below) P5CS were obtained from just 200 mL of insect cell culture. The MBP tag was crucial for P5CS solubility, although tag removal was essential for eliciting P5CS activity (data not shown).

Production of mutant forms of P5CS

The p.Arg371Gln and the p.Ser497Asn novel P5CS mutations (reported here in a new SPG9B family, see below) caused no gross P5CS misfolding, since both mutant forms were produced and purified with similar yield as wild-type P5CS (Fig. 1B, bottom image and yield below). Similar success was obtained in a prior study[2] with the pilot application of this method (without describing it) to the p.Val243Leu and p.Arg252Gln mutations found in SPG9A families. Thus, in principle, it appears that this procedure has general value for generating any clinical P5CS missense mutation.

The novel SPG9B mutations p.Arg371Gln and p.Ser497Asn decrease but do not abolish P5CS activity

p.Arg371Gln and p.Ser497Asn did not abolish P5CS activity although both of them caused 75–80% decreases in this activity (Fig. 1B, P5CS activity below gel image). These decreases in activity account for disease causation. They also show that the SPG9B phenotype is associated with a substantial level of residual P5CS activity. In contrast, some patients with the *ALDH18A1*-caused cutis laxa phenotype carried biallelic null mutations and exhibited total absence of P5CS protein.[7,8]

In agreement with the mapping of the mutations in the G5PR component of P5CS, these mutations did not substantially affect the G5K partial activity (Fig. 1B, G5K activity below gel image). In fact, they selectively decreased approximately fivefold the G5PR partial activity measured at saturation of any of the two substrates of this reaction, G5P and NADPH (Fig. 1C, values at high concentrations of these substrates; G5P levels are proportional to the amount of EcG5K added, see Supplementary Methods). As K_m values for these two substrates were not increased (Fig. 1C), the decrease in the activity was purely a V_{max} effect.

None of these two mutations affected importantly P5CS thermal stability, since although they decreased T_m values, the decrease was quite small (1–2°C, Fig. 1D).

Structure-based rationalization of the mutations' effects

The failure of the p.Arg371Gln and p.Ser497Asn mutations to increase the K_m values for G5P and NADPH in the G5PR reaction agrees with the mapping of Arg371 or Ser497 in the structure of the G5PR component of P5CS, away from the inferred binding sites for these substrates (Fig. 1E, upper panel). The magnitude of the decrease in V_{max} due to the mutations militates against a catalytic role of Arg371 and Ser497, two residues that sit far from the catalytic Cys612 (Fig. 1E, upper panel). It fits better the triggering by the mutations of more indirect effects, possibly due to changes in the equilibrium and/or the kinetics for the opening and closing of the two globular domains of the G5PR component inferred to take place during catalysis.[20] By making a salt bridge with Asp715 of the other subunit of the G5PR dimer (Fig. 1E, bottom panel), Arg371 stabilizes the open conformation. The Arg371Gln substitution abolishes such salt bridge and prevents this stabilization. Ser497 sits at the junction of the cofactor-binding domain, the catalytic domain and the oligomerization domain of the G5PR component (Fig. 1E, upper panel). This serine makes hydrophobic interactions in the interdomain regions that involve the

Table 1. Summary of the characteristics and in silico predictions for the mutations identified in our SPG9B patients.

Nucleotide change[1]	Protein change[2]	Amino acid in P5CS or in isolated microbial G5PR[3]			Domain of G5PR component	Pathogenicity server prediction				Base conservation
						Polyphen 2[4]		MutPred2[5]	Mutation taster 2[6]	PhyloP[7]
		Animals	Plants	Microbial		Prediction	Score	Score		Score
c.1112G> A	p.Arg371Gln	R	R	R/k	cofactor binding	Probably damaging	1	0.623	Disease-causing	5.035
c.1490G> A	p.Ser497Asn	S/t	S	S/t	cofactor binding	Probably damaging	1	0.791	Disease-causing	2.746

[1]GeneBank (https://www.ncbi.nlm.nih.gov/nucleotide/) reference sequences for human *ALDH18A1* gene, its mRNA (isoform 1, long form) and protein (long form), NG_012258.1, NM_002860.3 and NP_002851.2, respectively. Nucleotide numbering uses + 1 as the A of the ATG translation initiation codon (codon1).

[2]Uniprot KB (https://www.uniprot.org/uniprot/) reference number P54886.

[3]Amino acid conservation was determined by sequence alignment using Clustal, (https://www.ebi.ac.uk/Tools/msa/clustalo) of either P5CS from animals or plants or microbial G5PR from 45, 30 or 20 species, respectively. Residues in single letter amino acid code. Non-capitalized letters denote occurrence in low frequency.

[4]Polyphen-2 (HumVar-trained dataset; http://genetics.bwh.harvard.edu/pph2) grades the probability of a damaging effect of an amino acid change, as *probably damaging*, *possibly damaging* and *benign*. Highest probability score is 1.

[5]The score given by MutPred2 (http://mutpred2.mutdb.org) is the probability that a given amino acid change is deleterious/disease associated.

[6]http://www.mutationtaster.org

[7]PhyloP measures evolutionary conservation at individual alignment sites providing positive scores at sites that are predicted to be conserved (maximum 6) or negative scores (mínimum −14) when sites are predicted to evolve fast. The PhyloP result was taken from the report made by Mutation Taster

beginning of the protruding oligomerization domain (detailed in the middle panel of Fig. 1E), holding together these elements and anchoring them on the cofactor-binding domain. Mutation to Asn could disturb this anchoring, perhaps altering the dynamics rather than the equilibrium between open and closed forms.

A novel family presenting the recessive form of ALDH18A1-related spastic paraplegia

We diagnosed SPG9B in a 37-year-old male (see details in Supplementary Results) referred to us for a history of slowly progressive gait and motor disability due to spastic paraplegia, which led him over many years to the use of a walker and, from his mid-thirties, of a wheelchair. The patient showed intellectual disability, microcephaly, short stature, dysmorphic features (predominating facial ones), and irritative electroencephalographic findings. *ALDH18A1* missense mutations in compound heterozygosity were identified by WES and were confirmed by Sanger sequencing (Fig. S2). A brother of the patient showing a similar phenotype with onset at 3 years of age, in addition presenting seizures, was proven by Sanger sequencing to carry the same mutations as his brother. Each parent was confirmed for one variant, while a sister did not carry either (Fig. 2A). Family history was negative for intellectual or motor disabilities.

The *ALDH18A1* variants identified in the patients (Table 1) were c.1112G>A and c.1490G>A. The first, c.1112G>A, p.(Arg371Gln), affects a CpG island (hypermutable islands) and was found in heterozygous state in 7 out of 282,858 alleles in the GnomAD database. The second, c.1490G>A, p.(Ser497Asn), was unreported in databases. Both mutations were absent from our local database of WES data for nearly 1000 individuals. Neither was predicted to affect splicing (Human Splicing Finder server, http://www.umd.be/HSF3). Pathogenicity of the variants was supported by low or no presence of these variants in genomic variation databases, conservation of the bases (PhyloP scores, Table 1) and amino acids at these positions (Fig. 2B), and by unanimous predictions of disease causation by PolyPhen2, MutPred2, and MutationTaster 2 (Table 1), and, finally, by the above-reported experimental assays with the recombinantly produced protein.

Higher severity of SPG9B than of SPG9A

Our report of a further SPG9B family enlarges the family/patient/mutation database (Figs. 1A and 2C), and provides more evidence and insight into the correlation of the SPG9A and SPG9B phenotypes with their associated genotypes (Fig. 2C). These comparisons (Fig. 2C and D) strongly suggest that SPG9A, caused by dominant mutations, exerts less severe effects that the combined effects of the two recessive mutations found in SPG9B patients, who generally exhibit an earlier onset (Fig. 2D) and a progression to higher disability than SPG9A patients (Fig. 2C). They invariably present cognitive impairment and,

frequently, short stature, microcephaly, seizures, and dysmorphic features. These features have been reported less frequently or not at all in SPG9A patients (Fig. 2C). Only early cataracts seems to be more frequent in SPG9A than in SPG9B (Fig. 2C); however, more case reports would be needed to draw conclusions regarding cataract frequency.

Conclusions

The in vitro P5CS production system reported here is a highly useful tool to clarify the effects of individual P5CS mutations and thus to establish the molecular mechanisms of disease causation in *ALDH18A1*-related disorders. The use of this system has shown that the novel P5CS mutations p.Arg371Gln and p.Ser497Asn reported here in a new SPG9B family are disease causing, importantly decreasing P5CS enzyme activity. However, since they do not completely inactivate this enzyme, SPG9B is associated to partial rather than total P5CS deficiency. With the increased SPG9B family/patient database after addition of this new family, the dominant and recessive form of SPG9 can be compared on sound bases, leading to the conclusion that SPG9B is more severe than SPG9A, having a lower onset age, attaining greater disability, presenting constant impairment of cognition and more frequent growth restriction and dysmorphic traits.

Acknowledgments

We thank Nick S Berrow (IRB-Parc Cientific, Barcelona) and Prof. Ian M Jones (University of Reading, UK) for the DH10:KO1629 bacmid, and patients and family members who participated in this study, as well as the American Spastic Paraplegia Foundation for the EP grant "Understanding Hereditary Spastic Paraplegia: in vivo models to identify pathogenetic mechanism and therapeutic targets for SPG9," which was partially used for the research in this work. Whole-exome sequencing analysis was funded by a "Fondazione del Monte" grant to Professor MS for clinical exome sequencing applied to the diagnosis of ultrarare/orphan inherited diseases. The Genetic Bank (Biobanca del Laboratorio di Genetica Umana IRCCS Gaslini), member of the Network Telethon of Genetic Biobanks (Project No. GTB12001), funded by Telethon Italy, provided us with specimens. VR was supported by grants of the Fundación Inocente Inocente and of the Spanish Government (MINECO BFU2017-84264-P).

Conflict of Interest

The authors declare that they do not have any commercial or financial conflict of interests.

Authors Contributions

MS, EP, and VR conceived and designed the study; PM contributed with the Exome Sequencing and data analysis; CM-M, JME-H, and VR produced and functionally characterized P5CS, either wild-type or mutant, and carried out the structural analysis; FF, FF, DM, and CDV contributed to the patients clinical description and analysis of results. EP, MS, VR, and CM-M wrote the manuscript, and all the authors read it and made contributions to improve its writing.

References

1. Coutelier M, Goizet C, Durr A, et al. Alteration of ornithine metabolism leads to dominant and recessive hereditary spastic paraplegia. Brain 2015;138:2191–2205.
2. Panza E, Escamilla-Honrubia JM, Marco-Marín C, et al. *ALDH18A1* gene mutations cause dominant spastic paraplegia SPG9: loss of function effect and plausibility of a dominant negative mechanism. Brain 2016;139:e3.
3. Hu CA, Lin WW, Valle D. Cloning, characterization, and expression of cDNAs encoding human Δ^1-pyrroline-5-carboxylate dehydrogenase. J Biol Chem 1996;271:9795–9800.
4. Jones ME. Catalysts of the urea cycle. Trans N Y Acad Sci 1983;41:77–82.
5. Baumgartner MR, Hu CA, Almashanu S, et al. Hyperammonemia with reduced ornithine, citrulline, arginine and proline: a new inborn error caused by a mutation in the gene encoding Δ^1-pyrroline-5-carboxylate synthase. Hum Mol Genet 2000;9:2853–2858.
6. Baumgartner MR, Rabier D, Nassogne MC, et al. Δ^1-Pyrroline-5-carboxylate synthase deficiency: neurodegeneration, cataracts and connective tissue manifestations combined with hyperammonaemia and reduced ornithine, citrulline, arginine and proline. Eur J Pediatr 2005;164:31–36.
7. Skidmore DL, Chitayat D, Morgan T, et al. Further expansion of the phenotypic spectrum associated with mutations in *ALDH18A1*, encoding Δ^1-pyrroline-5-carboxylate synthase (P5CS). Am J Med Genet A. 2011;155A:1848–1856.
8. Fischer B, Callewaert B, Schröter P, et al. Severe congenital cutis laxa with cardiovascular manifestations due to homozygous deletions in *ALDH18A1*. Mol Genet Metab 2014;112:310–316.
9. Kremer LS, Bader DM, Mertes C, et al. Genetic diagnosis of mendelian disorders via RNA sequencing. Nat Commun 2017;8:15824.
10. Bicknell LS, Pitt J, Aftimos S, et al. A missense mutation in *ALDH18A1*, encoding Δ^1-pyrroline-5-carboxylate synthase (P5CS), causes an autosomal recessive neurocutaneous syndrome. Eur J Hum Genet 2008;16:1176–1186.

11. Martinelli D, Häberle J, Rubio V, et al. Understanding pyrroline-5-carboxylate synthetase deficiency: clinical, molecular, functional, and expression studies, structure-based analysis, and novel therapy with arginine. J Inherit Metab Dis 2012;35:761–776.
12. Fischer-Zirnsak B, Escande-Beillard N, Ganesh J, et al. Recurrent de novo mutations affecting residue Arg138 of pyrroline-5-carboxylate synthase cause a progeroid form of autosomal-dominant cutis laxa. Am J Hum Genet 2015;97:483–492.
13. Sivera R, Frasquet M, Lupo V, et al. Distribution and genotype-phenotype correlation of GDAP1 mutations in Spain. Sci Rep 2017;7:6677.
14. Steenhof M, Kibæk M, Larsen MJ, et al. Compound heterozygous mutations in two different domains of *ALDH18A1* do not affect the amino acid levels in a patient with hereditary spastic paraplegia. Neurogenetics 2018;19:145–149.
15. Koh K, Ishiura H, Japan Beppu M, et al. Spastic Paraplegia Research Consortium. Novel mutations in the *ALDH18A1* gene in complicated hereditary spastic paraplegia with cerebellar ataxia and cognitive impairment. J Hum Genet 2018;63:1009–1013.
16. Zhao Y, Chapman DA, Jones IM. Improving baculovirus recombination. Nucleic Acids Res 2003;31:E6.
17. Berrow NS, Alderton D, Sainsbury S, et al. A versatile ligation-independent cloning method suitable for high-throughput expression screening applications. Nucleic Acids Res 2007;35:e45.
18. Diez-Fernandez C, Martínez AI, Pekkala S, et al. Molecular characterization of carbamoyl-phosphate synthetase (CPS1) deficiency using human recombinant CPS1 as a key tool. Hum Mutat 2013;34:1149–1159.
19. Vedadi M, Niesen FH, Allali-Hassani A, et al. Chemical screening methods to identify ligands that promote protein stability, protein crystallization, and structure determination. Proc Natl Acad Sci USA 2006;103:15835–15840.
20. Page R, Nelson MS, von Delft F, et al. Crystal structure of gamma-glutamyl phosphate reductase (TM0293) from *Thermotoga maritima* at 2.0 Å resolution. Proteins 2004;54:157–161.

Supporting Information

Additional supporting information may be found online in the Supporting Information section at the end of the article.

Figure S1. Scheme of pOPINM-P5CS.
Figure S2. Validation of the two novel *ALDH18A1* mutations through Sanger sequencing in one of the two patients.

